JOURNAL OF MATERIALS SCIENCE **36** (2001) 1105–1117

Ceria-based materials for solid oxide fuel cells

V. V. KHARTON*‡
Institute of Physicochemical Problems, Belarus State University, 14 Leningradskaya Str., 220080 Minsk, Republic of Belarus
E-mail: kharton@cv.ua.pt; kharton@fhp.bsu.unibel.by

F. M. FIGUEIREDO
Dept. de Eng[a]. Cerâmica e do Vidro, UIMC, Universidade de Aveiro, 3810-193 Aveiro, Portugal; Dept. Ciências Exactas Tecnológicas, Universidade Aberta, R. Escola Politécnica 147, 1269-001 Lisboa, Portugal

L. NAVARRO
Dept. de Eng[a]. Cerâmica e do Vidro, UIMC, Universidade de Aveiro, 3810-193 Aveiro, Portugal

E. N. NAUMOVICH, A. V. KOVALEVSKY, A. A. YAREMCHENKO, A. P. VISKUP
Institute of Physicochemical Problems, Belarus State University, 14 Leningradskaya Str., 220080 Minsk, Republic of Belarus

A. CARNEIRO, F. M. B. MARQUES, J. R. FRADE
Dept. de Eng[a]. Cerâmica e do Vidro, UIMC, Universidade de Aveiro, 3810-193 Aveiro, Portugal

This paper is focused on the comparative analysis of data on electronic and ionic conduction in gadolinia-doped ceria (CGO) ceramics as well as on the electrochemical properties of various oxide electrodes in contact with ceria-based solid electrolytes. Properties of electrode materials, having thermal expansion compatible with that of doped ceria, are briefly reviewed. At temperatures below 1000 K, $Ce_{0.90}Gd_{0.10}O_{2-\delta}$ (CGO10) was found to possess a better stability at reduced oxygen pressures than $Ce_{0.80}Gd_{0.20}O_{2-\delta}$ (CGO20). Incorporation of small amounts of praseodymium oxide into $Ce_{0.80}Gd_{0.20}O_{2-\delta}$ leads to a slight improvement of the stability of CGO20 at intermediate temperatures, but the difference between electrolytic domain boundaries of the Pr-doped material and CGO10 is insignificant. Since interaction of ceria-based ceramics with electrode materials, such as lanthanum-strontium manganites, may result in the formation of low-conductive layers at the electrode/electrolyte interface, optimization of electrode fabrication conditions is needed. A good electrochemical activity in contact with CGO20 electrolyte was pointed out for electrodes of perovskite-type $La_{0.8}Sr_{0.2}Fe_{0.8}Co_{0.2}O_{3-\delta}$ and $LaFe_{0.5}Ni_{0.5}O_{3-\delta}$, and $LaCoO_{3-\delta}/La_2Zr_2O_7$ composites; surface modification of the electrode layers with praseodymium oxide results in considerable decrease of cathodic overpotentials. Using highly-dispersed ceria for the activation of SOFC anodes significantly improves the fuel cell performance.

1. Introduction

Solid electrolytes based on doped cerium dioxide, $Ce(M)O_{2-\delta}$ (M : rare-earth or alkaline-earth cations), are of considerable interest for potential use in solid oxide fuel cells (SOFCs) due to a higher ionic conductivity with respect to stabilized zirconia and a lower cost in comparison with lanthanum gallate-based phases [1–5]. High oxide ion conduction in doped ceria makes it possible to decrease SOFC operation temperature, thus reducing numerous technological problems. Among ceria-based ionic conductors, the highest level of oxide ion conductivity is characteristic of the solid solutions $Ce_{1-x}M_xO_{2-\delta}$, where M = Gd or Sm, $x = 0.10$–0.20. Other promising applications of doped ceria refer to SOFC anode materials, solid-electrolyte oxygen pumps and mixed-conductive membranes for oxygen separation and partial oxidation of hydrocarbons [6–10]. For membrane applications, significant oxygen permeability of $CeO_{2-\delta}$ may be achieved either by dissolution of variable-valence metal oxides in the cerium dioxide lattice or by dispersion of an electronically-conducting phase in the ceria matrix [6, 10–12].

The main disadvantages of doped $CeO_{2-\delta}$ ceramics are associated with a relatively easy reducibility at low oxygen partial pressures, which leads to increasing electronic transport and possible mechanical

*Author to whom all correspondence should be addressed.
‡*Present Address*: Dept. de Eng[a]. Cerâmica e do Vidro, UIMC, Universidade de Aveiro, 3810-193 Aveiro, Portugal.

decomposition under large oxygen chemical potential gradients typical of SOFC operation [1, 2, 5, 7, 13, 14]. Such problems can be partially solved by decreasing the operating temperature of the electrochemical cells to values below 920–970 K, or by a combination of $Ce(M)O_{2-\delta}$ with other solid electrolytes such as stabilized zirconia or doped lanthanum gallate, in multi-layer cells [5, 13–16]. However, the performance of multi-layer cells is relatively poor due to the formation of layers with low conductivity at the interface between the solid-electrolyte phases as well as differences in thermal expansion of the electrolytes, resulting in microcracks [15–17]. In the case of reduced operating temperature, polarization resistance of electrodes becomes critical, decreasing the performance, while local heating due to non-uniform current and/or reaction rate distribution along the solid-electrolyte membrane may still result in irreversible decomposition of ceria-based ceramics. This requires further modification of ceria-based electrolytes in order to improve their stability, and development of novel electrode materials with high electrochemical activity.

The present work represents a brief summary of our continuous research on transport and electrochemical properties of $CeO_{2-\delta}$-based oxides, partly published elsewhere [11, 12, 18–24]. Particular emphasis is given to electrode materials having thermal expansion coefficients compatible with that of doped ceria.

2. Materials and measurement techniques

Experimental techniques used for preparation and characterization of solid solutions $Ce(Gd)O_{2-\delta}$ (CGO) and $Ce(Gd, Me)O_{2-\delta}$ (Me = Pr, Mn, Co), including X-ray diffraction (XRD), scanning electron microscopy (SEM), analysis of cation composition and dilatometry, were described elsewhere [11, 12, 19–24]. Compositions studied in this work and corresponding abbreviations are listed in Tables I and II. The transport properties were tested using impedance spectroscopy (IS), 4-probe DC conductivity measurements, determination of steady oxygen permeation fluxes (OP), e.m.f. of oxygen-concentration cells (EMF), the Faradaic efficiency method (FE) and electrochemical cells employing an ion-blocking electrode (BE). Detailed descriptions of these measurement techniques were published earlier [11, 19–27]. Unless otherwise specified, the presented data on bulk properties of solid electrolytes and mixed conductors (conductivity, oxygen permeability, transference numbers, thermal expansion) corresponds to single-phase gas-tight ceramics, having no less than 93% of the theoretical density. The techniques for fabrication of electrode layers, study of electrochemical properties and testing of single solid oxide fuel cells were reported in [22, 24, 28, 29] and references therein. For electrode materials studied in contact with CGO electrolytes, this paper contains references to our original publications devoted to their detailed characterization.

3. Results and discussion

3.1. Ionic conductivity of gadolinia-doped ceria

Ceria-based ceramics with various microstructures studied by impedance spectroscopy confirmed the conclusion [39] that the grain boundary contribution to the total conductivity of CGO decreases with increasing average grain size for grain sizes larger than 2-3 μm, whilst the grain conductivity of the materials prepared by a similar route is essentially independent of grain dimensions. As an example, Fig. 1 shows impedance spectra of CGO20 ceramics obtained after pressing and sintering a commercial powder, prepared by Praxair Specialty Chemicals (Seattle), for 2 hours at 1773 and 1873 K, in air. SEM micrographs illustrating the respective microstructures are given in Fig. 2. Increasing sintering temperature leads to an obvious increase in the grain size. This is accompanied by decreasing grain boundary resistivity, which may be estimated from the width of the intermediate-frequency semicircle in the impedance spectra. The grain interior contribution is kept similar, independent of the sintering conditions.

TABLE I Abbreviations, XRD data and thermal expansion coefficients (TECs) of $CeO_{2-\delta}$-based ceramics

Composition	Abbreviation	Phase composition*	Fluorite unit cell parameter, (nm)	Average TECs (300–1100 K)	
				Measurement method**	$\bar{\alpha} \times 10^6$, K^{-1}
$Ce_{0.90}Gd_{0.10}O_{2-\delta}$	CGO10	F	0.5417	XRD	13.4 ± 0.1
$Ce_{0.80}Gd_{0.20}O_{2-\delta}$	CGO20	F	0.5425	D	11.8 ± 0.1
$Ce_{0.80}Gd_{0.18}Pr_{0.02}O_{2-\delta}$	CGO18Pr2	F			
$Ce_{0.75}Gd_{0.20}Mn_{0.05}O_{2-\delta}$	CGO20Mn5	F	0.5421		
$Ce_{0.70}Gd_{0.20}Mn_{0.10}O_{2-\delta}$	CGO20Mn10	F + Mn	0.5421		
$Ce_{0.60}Gd_{0.20}Mn_{0.20}O_{2-\delta}$	CGO20Mn20	F + Mn	0.5420	D	13.3 ± 0.9
$Ce_{0.88}Gd_{0.10}Co_{0.02}O_{2-\delta}$	CGO10Co2	F	0.5415	XRD	12.9 ± 0.1
				D	11.7 ± 0.1
$Ce_{0.85}Gd_{0.10}Co_{0.05}O_{2-\delta}$	CGO10Co5	F	0.5416	D	12.2 ± 0.1
$Ce_{0.80}Gd_{0.10}Co_{0.10}O_{2-\delta}$	CGO10Co10	F	0.5417	XRD	13 ± 1
				D	12.4 ± 0.4
$Ce_{0.75}Gd_{0.10}Co_{0.15}O_{2-\delta}$	CGO10Co15	F + Co	0.5417	D	13.9 ± 0.3
$Ce_{0.70}Gd_{0.10}Co_{0.20}O_{2-\delta}$	CGO10Co20	F + Co	0.5417	D	14.2 ± 0.2
$Ce_{0.60}Gd_{0.10}Co_{0.30}O_{2-\delta}$	CGO10Co30	F + Co			

* "F", "Mn" and "Co" correspond to the fluorite, manganese and cobalt oxide phases, respectively.

** "XRD" and "D" refer to the high-temperature XRD analysis and dilatometric measurements, respectively.

TABLE II Properties of electrode materials having TECs compatible with thermal expansion of CGO

Compositions and abbreviations	Average TEC		Total conductivity		Oxygen permeability (0.21/0.021 atm O_2)		Detailed information
	T, K	$\bar{\alpha} \times 10^6$, K^{-1}	T, K	σ, S/cm	T, K	$J(O_2)$ (mol × s^{-1} × cm^{-1})	
$La_{0.7}Sr_{0.3}MnO_{3-\delta}$ (LSM30)	300-1100	11.7 ± 0.1	873 1123	190 200	1223	1.6×10^{-12}	[11]
$La_{0.6}Sr_{0.4}Mn_{0.8}Ni_{0.2}O_{3-\delta}$ (LSMN)	300-1100	12.7 ± 0.1	873 1123	150 170	1223	$<1 \times 10^{-12}$	[30]
$La_2Zr_2O_7/LaCoO_{3-\delta}$ (LZ/LC) composite (41 vol% LC)	300-1100	13.7 ± 0.1	873 1123	160 250	1223	$<1 \times 10^{-10}$	[22, 24, 31]
CGO20/LSM30 composite (48 vol% CGO)	300-1100	11.7 ± 0.1	873 1123	32 33	1223	2.7×10^{-9}	[11]
$LaFe_{0.5}Ni_{0.5}O_{3-\delta}$ (LFN)	300-1100	11.9 ± 0.1	873 1123	830 680	1223	3.6×10^{-10}	[32]
$LaGa_{0.5}Ni_{0.5}O_{3-\delta}$	300-1100	11.4 ± 0.3	873 1123	25 28	1223	2.9×10^{-9}	[33]
$LaGa_{0.4}Ni_{0.6}O_{3-\delta}$*	300-1100	11.3 ± 0.1	873 1123	220 270	1223	8.3×10^{-10}	[33]
$SrCo_{0.7}Ni_{0.3}O_{3-\delta}$**	300-1100	13.0 ± 0.3	873 1123	16 20	1123	6.4×10^{-9}	[34, 35]
$La_{0.8}Sr_{0.2}Fe_{0.8}Co_{0.2}O_{3-\delta}$*** (LSFC)	470-1070	15.4 [36]	1123	180 [36]	1123	2.1×10^{-10}	[24, 37]
$La_{1.9}Sr_{0.1}Ni_{0.98}Fe_{0.02}O_{4+\delta}$	300-1100	12.5 ± 0.1	873 1123	81 64	1123	1.8×10^{-9}	[27]
$La_2Ni_{0.88}Fe_{0.02}Cu_{0.10}O_{4+\delta}$	300-1100	10.5 ± 0.2	873 1123	44 33	1123	3.7×10^{-9}	[27]
$La_2Cu_{0.98}Co_{0.02}O_{4+\delta}$	470-1050	12.2 ± 0.3	873 1123	14 12	1123	1.2×10^{-9}	[38]
$La_2Cu_{0.70}Co_{0.30}O_{4+\delta}$****	470-1070	12.6 ± 0.2	873 1123	5.5 8.1	1123	2.3×10^{-9}	[38]

* thermodynamically unstable in air at temperatures above 1170 K.
** non-single-phase material.
*** the conductivity and TEC values are taken from Ref. [36].
**** thermodynamically unstable in air at temperatures below approximately 1200 K.

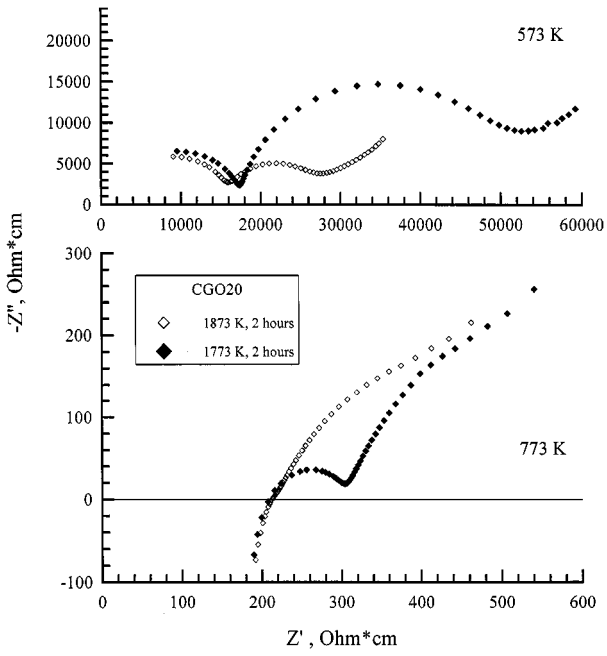

Figure 1 Complex impedance spectra of CGO20 ceramics sintered in air at 1873 and 1773 K for 2 hours.

Fig. 3 shows temperature dependencies of the total conductivity of selected CeO_2-based ceramics in air. For solid-electrolyte materials such as CGO10, CGO20 and CGO18Pr2, the grain bulk conductivity values are given. For transition-metal doped compositions where separation of the grain and grain boundary contributions is complicated due to a relatively high electronic conduction, Fig. 3 presents the total conductivity values without corrections for grain boundary contribution. The lattice conductivity of CGO10, CGO20 and CGO18Pr2 ceramics, determined by IS, are close to each other. Substitution of 2% Gd with Pr in CGO20 has little effect on ionic conduction—only a slight increase in the conductivity of CG18Pr2 with respect to CGO20 is observed at temperatures above 870 K. This behavior is in agreement with the literature data [40, 41], and can be understood because of the small amount of praseodymium oxide added. In fact, the maximum ionic conductivity in fluorite-type oxides is observed when the dopant ion radius is close to the radius of host cations, resulting in a lower enthalpy for association of oxygen vacancies and dopant ions [1, 3]. Since Gd^{3+} ions are larger than Ce^{4+}, the average dopant radius could be matched using a second dopant such as Y^{3+} [42]; additions of Pr^{4+} into CGO might also lead to a higher conductivity. However, small additions of several cations for improving ionic transport seem to be ineffective, probably due to segregation of dopants at the grain boundaries [1].

When comparing the conductivity of CGO10 and CGO20, one should note that the identification of the exact composition in the CeO_2-Gd_2O_3 system, having a maximum conductivity, is still under discussion (for instance, compare data in refs.[1, 3, 4, 43]) and is probably

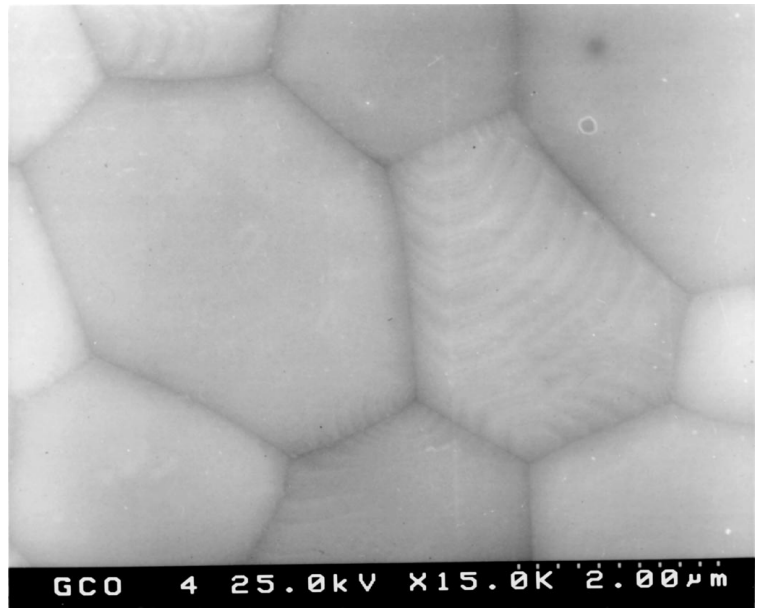

(A)

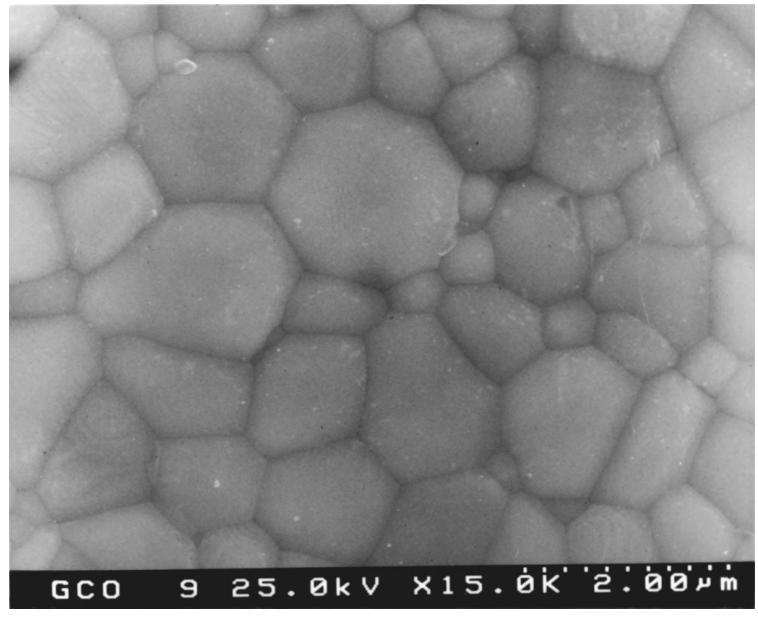

(B)

Figure 2 SEM micrographs of CGO20 ceramics sintered in air at 1873 (A) and 1773 K (B) for 2 hours.

between 10 and 20 mol% of $GdO_{1.5}$. Steele [1] reported a lower grain boundary and higher lattice conductivity of CGO10 in comparison with CGO20, which makes sufficiently pure CGO10 to be more appropriate for use in intermediate-temperature SOFCs. At the same time, the lattice conductivity, obtained from impedance spectroscopy assuming the "brick layer" model, may be significantly affected by specific microstructural features, including porosity, nature of the grain boundaries and grain size [44]. Therefore, the identification of the most-conductive composition should be performed only after optimization of the preparation route in order to provide regular microstructures and low grain boundary resistances.

3.2. p-type electronic conductivity of CGO

The results of Faradaic efficiency tests of CGO20 ceramics under an oxygen pressure gradient of 1.0/0.21 atm are given in Table III. It is obvious that the error in the ion transference number determination using the Faradaic efficiency technique, which is no less than 2%, exceeds the electron transference number in CGO. This makes it impossible to study the

TABLE III Oxygen ion transference numbers of CGO20 estimated from the Faradaic efficiency data under the oxygen partial pressure gradient of 1.0/0.21 atm

Electrode	T, K	Current density, mA/cm^2	Ion transference number, t_o
Pt	1223	100.7	1.01*
		50.3	1.00
	1123	47.8	0.98
Ag	1023	35.4	1.00
	923	7.0	0.99
	823	1.2	1.02

*The values in excess of unit are due to the measurement error.

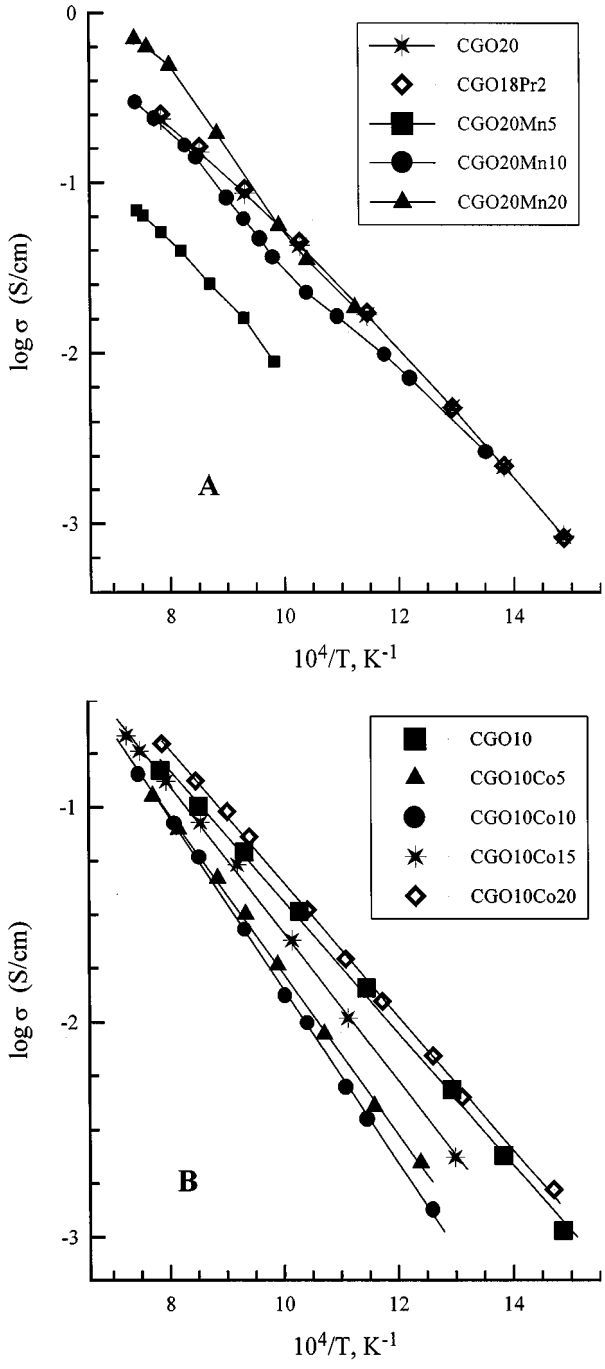

Figure 3 Temperature dependence of the total conductivity in air: (A), CGO20 and CGO20-based ceramics, (B), CGO10 and CGO10-based ceramics. The solid lines are for visual guidance only.

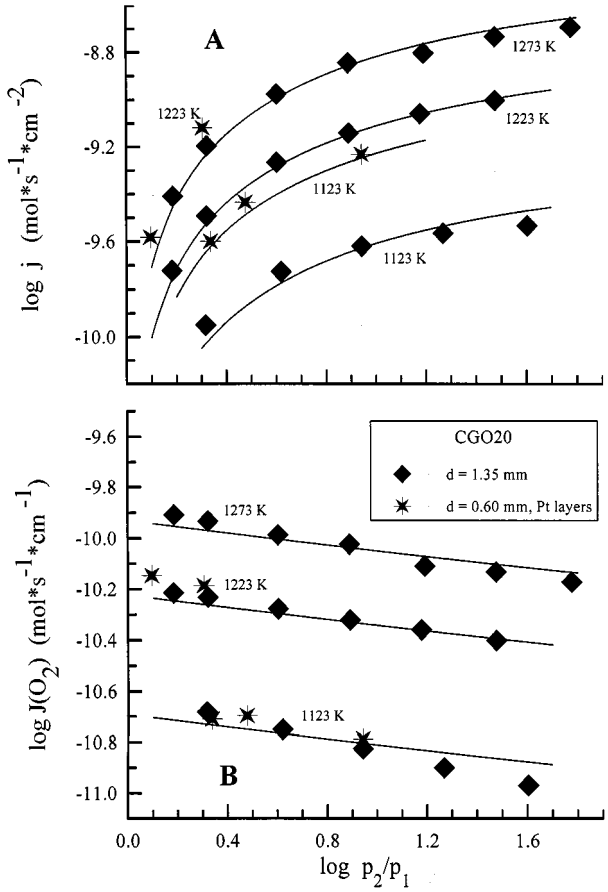

Figure 4 Dependence of the oxygen permeation flux density (A) and specific oxygen permeability (B) of CGO20 membranes on the oxygen partial pressure difference at $p_2 = 0.21$ atm. The solid lines correspond to fitting results using Equation 2 as regression model.

electronic conduction in gadolinia-doped ceria (an almost pure ionic conductor in oxidizing conditions) either by Faradaic efficiency measurement or by studying the oxygen partial pressure dependence of the total conductivity. The determination of the p-type electronic transport in oxidizing atmospheres was carried out using the oxygen permeation [21, 27] and modified e.m.f. [25] methods. In the case of oxygen permeability measurements, the permeation fluxes through CGO membranes at oxygen pressures close to air are limited by the electron hole conduction [23]. The modified e.m.f. method can be used to measure small electronic contributions choosing electrodes with a high polarization resistance; in this case the effect of electronic conductivity on the measured e.m.f. increases, and can be determined from the dependence of the cell voltage on external load resistance [25].

Fig. 4 shows the oxygen permeation flux density (j) and specific oxygen permeability ($J(O_2)$) of CGO20 membranes as functions of the oxygen pressure gradient. The values of the oxygen permeability were calculated using the formula [45]

$$J(O_2) = j \cdot d \cdot \left[\ln \frac{p_2}{p_1}\right]^{-1} \quad (1)$$

where d is the membrane thickness, p_2 and p_1 are the oxygen partial pressures at the membrane feed and permeate sides, respectively ($p_2 > p_1$). The oxygen permeability of gadolinia-doped ceria is independent of the membrane thickness within the limits of experimental error; deposition of porous platinum layers onto the membrane surface also has no effect on oxygen permeation (Fig. 4). Since $J(O_2)$ is proportional to $j \times d$ by definition, this behavior suggests negligible surface limitations to the oxygen permeation flux. Hence, the permeation is limited by the bulk ambipolar conductivity. When the oxygen ion transference numbers are close to unity (Table III), the ambipolar conductivity is close to the electronic one. Assuming that the oxygen vacancy concentration is independent of oxygen

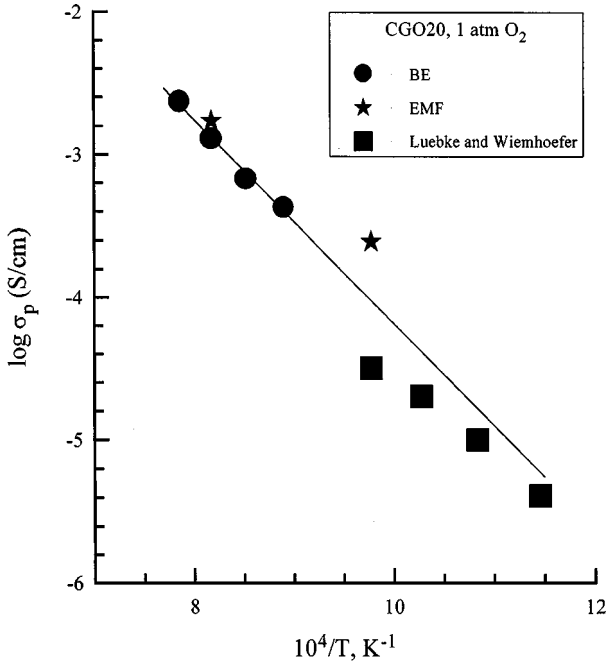

Figure 5 Temperature dependence of the p-type electronic conductivity of CGO20 at $p(O_2) = 1$ atm, calculated from the oxygen permeation results using Equation 2. The data [39] and the e.m.f. measurement results, obtained under oxygen pressure gradient of 1.0/0.21 atm, are given for comparison.

pressure, and that the p-type conductivity is proportional to $p(O_2)^{1/4}$, leads to the following simplified model for the oxygen permeation flux:

$$j = \frac{RT}{Fd} \cdot \sigma_p^0 \left(p_2^{1/4} - p_1^{1/4}\right) \tag{2}$$

where σ_p^0 is the value of the electron-hole conductivity at an oxygen partial pressure of 1 atm. The solid lines in Fig. 4 correspond to the best fit according to Equation 2. This model provides a sufficiently adequate description of the oxygen permeation process, suggesting the p-type conduction to be the permeation-limiting factor.

The temperature dependence of the electron-hole conductivity of CGO at $p(O_2) = 1$ atm, calculated from the oxygen permeability data, is given in Fig. 5. For comparison, Fig. 5 shows also the corresponding values, measured by the e.m.f. method under an oxygen pressure gradient of 1.0/0.21 atm, and the results of Ref. [41], obtained by the ion-blocking technique. In fact, all these data may be described by a single Arrhenius dependence.

3.3. n-type electronic conductivity of gadolinia-doped ceria

As for the electron-hole conduction, estimation of the n-type electronic conductivity was based on the simplest model, assuming $p(O_2)$-independent oxygen vacancy concentration and the direct proportionality between the electron concentration and $p(O_2)^{-1/4}$:

$$\sigma_n = \sigma_n^0 \cdot [p(O_2)]^{-1/4} \tag{3}$$

where σ_n^0 is the value of the electronic conductivity at unit oxygen pressure. Cells with ion-blocking electrodes were used for these measurements; calculations of the n-type conductivity were carried out using the Hebb- Wagner equation [18]. Electronic conduction in solid electrolytes determines their stability at low chemical potentials, which may be expressed in terms of the electrolytic domain boundary (P_e). The latter quantity corresponds to the oxygen partial pressure when the n-type electronic conductivity becomes equal to the ionic conductivity:

$$\sigma_n = \sigma_o \tag{4}$$

Respectively,

$$P_e = \left(\frac{\sigma_o}{\sigma_n^0}\right)^{-4} \tag{5}$$

Fig. 6 (A and B) presents a comparison of the electrolytic domain boundary, calculated from data obtained with ion-blocking electrodes [18], with the results of other authors [4, 40, 41, 46]. Except for the data of Yahiro *et al.* [46], the agreement between results is rather good taking into account the difference in measuring techniques.

The variation in the P_e values for CGO10, CGO20 and CGO18Pr2 in the studied temperature range was found to be within 2-3 orders of magnitude (Fig. 6B). At temperatures below 900 K, the CGO10 ceramics exhibit a better stability in reducing environments in comparison with CGO20. Consideration of these data in combination with the similar ionic conductivity values obtained for CGO10 and CGO20 (Fig. 3) supports the conclusion of Steele [1] that 10% gadolinia doped-ceria is preferable for intermediate-temperature SOFCs operating at 770 K.

The electrolytic domain boundary of CGO18Pr2 at $T > 1100$ K is close to that of CGO20. Decreasing temperature leads to lower P_e values of Pr-doped CGO, which tend to the level characteristic of CGO10 at temperatures below 900 K. One should note that the results obtained as well as the data in ref. [41] are relatively close to the observation of Maricle *et al.* [40], who reported a difference in the electrochemical domain boundary of $Ce_{0.80}Gd_{0.20}O_{2-\delta}$ and $Ce_{0.80}Gd_{0.17}Pr_{0.03}O_{2-\delta}$ at 973 K of about two orders of magnitude. Therefore, small additions of praseodymium oxide may indeed result in a moderate increase in stability of CGO20 at intermediate temperatures, as claimed by Maricle *et al.* [40, 47]. However, such an improvement is relatively small, and consideration of the higher p-type electronic conductivity of Pr-doped CGO [41] makes questionable the practical use of such materials.

Another important note is that the estimations of the electrolytic domain boundary based on the above- mentioned simplified assumptions may be considered only as crude approximations. Experimental and theoretical data (for example, [48, 49]) shows a non-negligible dependence of the ionic conductivity of doped ceria

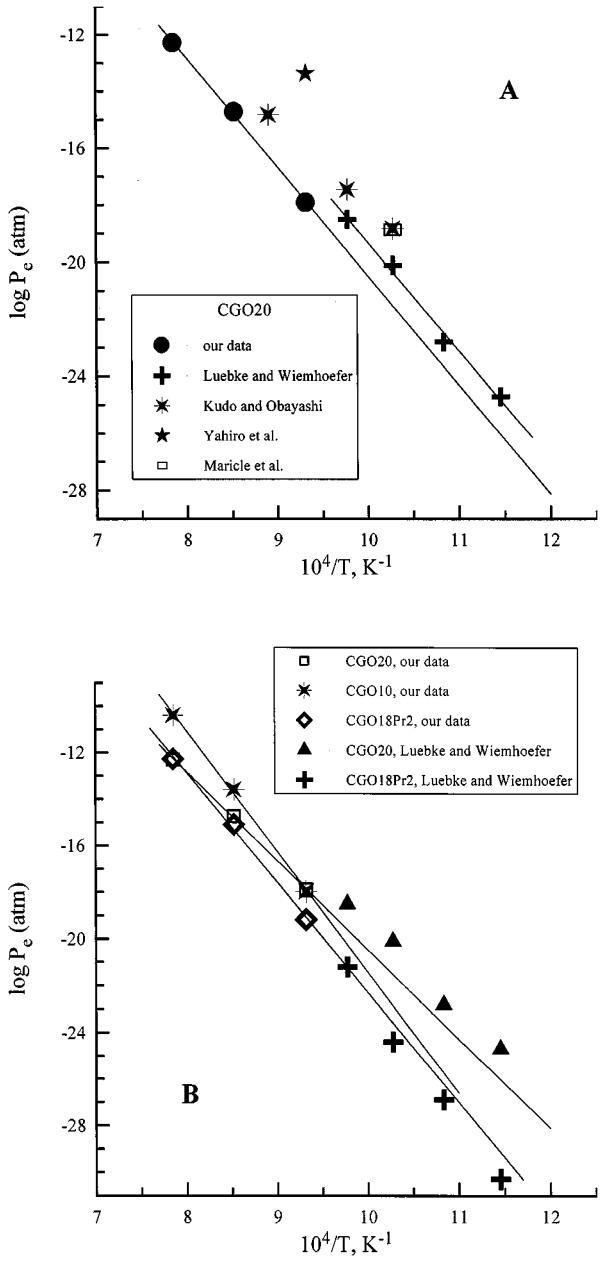

Figure 6 Temperature dependence of the electrolytic domain boundary of CeO_2-based electrolytes at low oxygen pressures.

on oxygen chemical potential at high oxygen nonstoichiometry values; the electronic conductivity in these conditions also does not follow the simplified dependence Equation 3. In addition, oxygen currents flowing through the fuel cell lead to increasing oxygen chemical potential at the anode, which may increase the stability of the electrolyte under SOFC operation conditions [5], with obvious benefit to the application domain of the materials.

The possible role of grain boundaries in the measured values of p- and n-type electronic conductivities should also be emphasised. The electrochemical techniques, including ion-blocking, e.m.f. of oxygen concentration cells and oxygen permeation measurement, do not allow separation of the grain boundary and bulk contributions to the measured quantities. However, the results obtained by these techniques make it possible to optimize composition and preparation route, and are thus mainly of interest for the practical applications of the ceramic materials.

3.4. Interaction of CGO with manganese and cobalt oxides and lanthanum-strontium manganite

XRD results on $Ce_{0.90-x}Gd_{0.10}Co_xO_{2-\delta}$ and $Ce_{0.80-x}Gd_{0.20}Mn_xO_{2-\delta}$ ceramics demonstrated that the solid solubility of cobalt and manganese oxides in the CGO lattice does not exceed 10 mol%. Therewith, the solid solution formation range in the case of manganese is more narrow with respect to cobalt; segregation of manganese oxide as a second phase was observed at $x = 0.10$, whereas 10 mol% Co doped CGO10 was single phase. These results are in good agreement with the data of Pound [50]. At the same time, it should be mentioned a significant dependence of the solid solution formation range in these systems on temperature. For example, quenching ceramics with the transition metal dopant content as large as 20–30 mol% resulted in forming single-phase ceramics at room temperature; these oxides were found to decompose for 30–60 days, leading to formation of two-phase mixtures of the fluorite-type solid solutions and manganese or cobalt oxides. Notice that the observed behavior and solid solubility ranges are quite close to those of stabilized zirconia doped with transition metal oxides [9].

The variation of the transport properties of ceria-based ceramics with additions of manganese and cobalt is also similar to the respective zirconia-based systems [9]. Doping with transition metal oxides leads to decreasing ionic conductivity and increasing electronic transport of ceria (Figs 3 and 7, [20, 21]). In particular, oxygen permeability of doped ceria significantly

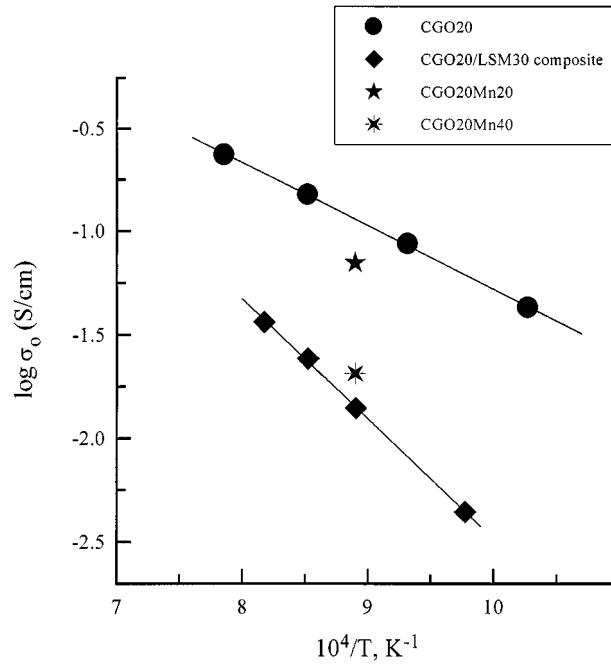

Figure 7 Temperature dependence of oxygen ionic conductivity of CeO_2-based ceramics. The results on CGO20 were obtained using impedance spectroscopy. Ionic conductivity of other materials was calculated from the oxygen permeation and total conductivity measurement data.

increases with increasing transition metal dopant content [11, 20, 21]. Taking into account the decrease in the total conductivity with manganese and cobalt additions (Fig. 3), such behaviour is unambiguously caused by increasing electronic transport. Here, the higher electronic conductivity is obviously due to hopping of electronic charge carriers between the variable-valence cations, while a decrease in the ionic conduction is probably related to blocking of oxygen vacancies and/or ions near the transition metal cations due to local distortions of the fluorite lattice. Within the solid solution formation ranges, incorporation of Co or Mn into CGO leads to greater oxygen permeation fluxes as a result of the higher p-type electronic conduction; segregation of the second phases was found to decrease oxygen permeability [12, 20, 21].

Studies of CGO20/LSM30 composite ceramics, containing approximately 48 vol% of the gadolinia-doped ceria phase (Table II), showed that ionic conductivity of these materials is relatively low and decreases with increasing temperature or time of sintering [11]. At the same time, the fluorite unit cell parameter of ceria increases with thermal treatments, indicating diffusion of lanthanum and strontium cations into the CGO grains. This behavior suggests a formation of low-conductive layers at the ceria/manganite interface, which block the ionic transport. Such layers may represent, firstly, the ceria-based phase with high lanthanum and strontium content; formation of $SrCeO_3$-based phases having a low oxygen ionic conductivity might also take place. As an example, Fig. 8 shows a clear pattern of degradation of CGO20/LSM30 composite membrane with time, resulting either from continuing interaction of ceria and lanthanum-strontium manganite at 1223 K or from segregation of $SrCeO_3$-based phase at the grain boundaries.

Therefore, interaction of CGO with electrode materials, containing lanthanum, strontium and transition metals, may lead to formation of low-conductive layers at the interface. While doping of ceria-based ceramics with small amounts of transition metal cations results in a higher oxygen permeability, moderate diffusion of these metals may be useful from viewpoint of increasing electrochemical activity. However, diffusion of lanthanum and strontium unambiguously leads to a degradation in transport properties and should be hence avoided. Thus, fabrication of the electrodes should be performed at possible minimum temperature in order to suppress interaction between ceria-based electrolytes and electrode materials.

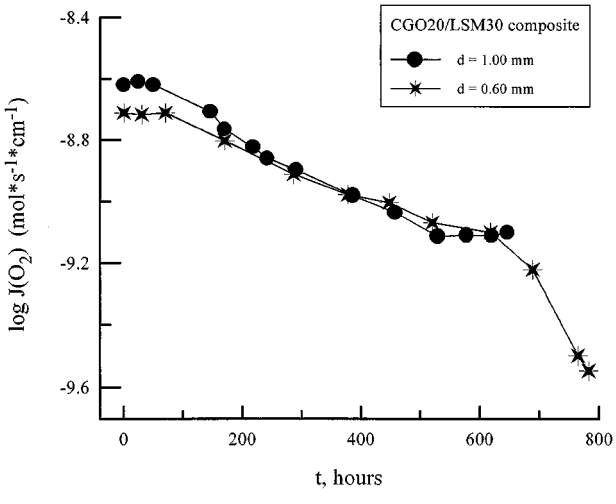

Figure 8 Time dependence of the oxygen permeability of CGO20/LSM30 composite membranes at 1223 K.

TABLE IV Thermal expansion coefficients of CGO20 ceramics with different porosity, calculated from dilatometric data and averaged in the temperature range 300–1100 K

d_{exp}/d_{theor}, %	$\bar{\alpha} \times 10^6$, K^{-1}	ρ
86	11.56 ± 0.09	0.9992
89	11.8 ± 0.1	0.9993
90	11.5 ± 0.1	0.9992
93	11.9 ± 0.1	0.9987
96	11.8 ± 0.1	0.9990

d_{exp}/d_{theor} is the ratio of the experimental and theoretical densities; ρ is the correlation coefficient of the linear model of thermal expansion.

3.5. Thermal expansion of CGO and respective electrode materials

Average thermal expansion coefficients (TECs) of CGO20 ceramics having various porosity are adduced in Table IV. In the studied range of apparent density, the TEC values are similar and vary in the range $(11.5–11.9) \times 10^{-6}$ K^{-1}; no dependence of thermal expansion on porosity was found. One should mention that the observed TECs are lower than the value of 12.5×10^{-6} K^{-1} reported by Mogensen *et al.* [43] for the temperature range of 323–1273 K. This is obviously caused by a narrower temperature range (300–1100 K) exploited in this work. Thermal expansion coefficients of doped ceria increase slightly with increasing temperature, and narrowing the total temperature range for the calculations leads to lower average TECs. For example, the thermal expansion coefficient of CGO20 ceramics (93% of the theoretical density), averaged in the temperature range 300–1233 K, was $(12.2 \pm 0.1) \times 10^{-6}$ K^{-1}, which is close enough to data in Ref. [43]. The temperature range used in the present work was chosen from a viewpoint that an analysis of compatibility of materials of the electrochemical cells should be performed using the quantities corresponding to real operation conditions; the operating temperature of SOFCs with ceria-based solid electrolytes should not exceed 1000 K.

Table II lists a number of electrode materials having TECs, more or less compatible with thermal expansion of gadolinia-doped ceria. All data on thermal expansion and transport properties of these materials were obtained by the authors, except for the conductivity and TEC of $La_{0.8}Sr_{0.2}Fe_{0.8}Co_{0.2}O_{3-\delta}$ (LSFC) where the data of Tai *et al.* [36] are used. The best compatibility with CGO from viewpoint of thermal expansion belongs to lanthanum-strontium manganites and solid solutions $La(Fe,Ni)O_{3-\delta}$; these perovskites, however, possess a relatively low oxygen ionic conductivity. Another interesting group of electrode materials refers to $La_2NiO_{4+\delta}$- and $La_2CuO_{4+\delta}$-based solid solutions with the K_2NiF_4-type structure; oxygen ionic transport in such oxides is much faster in comparison

with manganites. On the other hand, the higher concentration of A-site cations, such as lanthanum, in the K_2NiF_4-type oxide compounds leads to an expectation of greater diffusion of these cations into CGO, forming low-conductive layers at the electrode/electrolyte interface; this may complicate fabrication of electrodes. In addition, the Cu-containing K_2NiF_4-type oxides, having the lowest TECs, possess a relatively low melting point in the range 1300–1400 K.

3.6. Cathodic behavior of oxide electrodes in contact with doped ceria electrolyte

Selected results on cathodic polarization of porous electrodes of several studied materials in contact with CGO20 solid electrolyte are shown in Fig. 9. Curves 4 and 5 correspond to the $LaCoO_{3-\delta}/La_2Zr_2O_7$ (LC/LZ) composite cathodes, with 41 vol% of lanthanum cobaltite and different microstructures (Fig. 10). Two different electrode microstructures are presented: curve 4—a double layer structure (Fig. 10A) with a dense layer (thickness of about 12 μm) in direct contact with the electrolyte and a porous layer (24 μm) on top of it; curve 5—an electrode consisting of a single 48 μm thick porous layer (Fig. 10B). Details of the deposition techniques and electrode microstructures can be found in [22, 28–31] and references therein.

In general, as mentioned for ZrO_2- and Bi_2O_3-based solid electrolytes [51, 52], the bulk transport properties such as oxygen ionic or electronic conductivity of mixed-conductive electrodes in contact with gadolinia-doped ceria electrolyte are not the only parameters with relevance on electrode performance. This is particularly evident at high temperature when the increasing oxygen deficiency in the perovskites results in a significant increase in ionic conductivity, extending the electrode reaction from the electrode/electrolyte/gas triple-phase boundary to the electrode/gas interface. In such circumstances, the polarization resistance becomes strongly dependent of the electrode material surface characteristics, namely specific electrocatalytic activity and available surface area for oxygen reduction. For example, the LC/LZ composites possess a lower oxygen permeability than LSFC (Table II), but exhibit electrode performance similar to LSFC at 973–1073 K (Fig. 9). Comparison of both composite electrodes also suggest an electrode process limited at the electrode/gas phase interface, with the dense layer in direct contact with the electrolyte having no apparent effect on the electrochemical activity. Analogously, surface modification of LSMN electrodes affects remarkably the electrode performance, leading to the decrease of polarization. In fact, the cathodic polarization of the PrO_x-modified LSMN electrode is lower than the polarization of LSFC layers, whereas oxygen permeation of the lanthanum-strontium manganite-nickelate is negligible in comparison with LSFC.

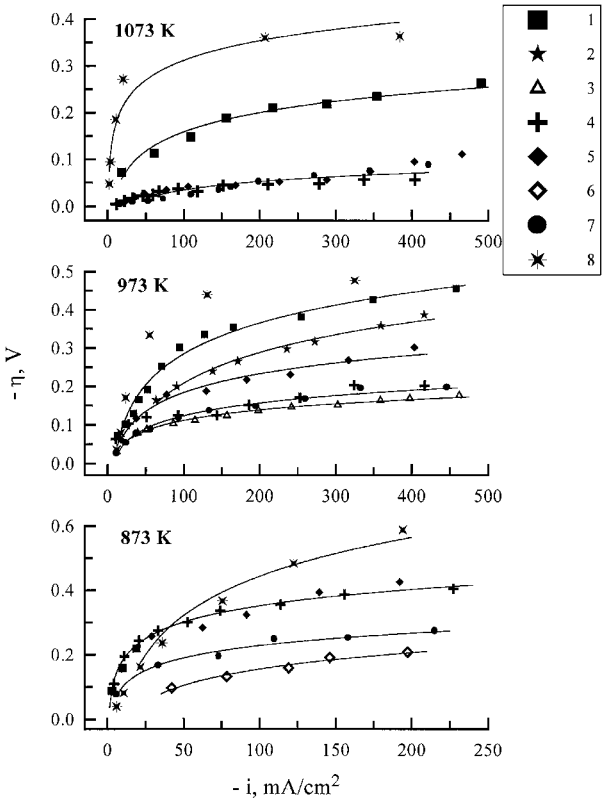

Figure 9 Dependence of cathodic overpotential of electrodes, applied onto CGO20 electrolyte, on current density in air: (1), LSM30; (2), LSMN after fabrication; (3), LSMN modified with PrO_x; (4), double layer dense plus porous LC/LZ composite; (5), single layer LC/LZ composite; (6), LFN activated with PrO_x and metallic silver; (7), LSFC; (8), Pt. Solid lines are a guide to the eye. The techniques of electrode surface modification were described in [28, 29].

The obtained results demonstrate evidence of an additional mechanism that could be related to the solid electrolyte surface properties. The measured overpotential vs. current dependence of the platinum cathode at 1073 K (curve 8) shows a significant increase of the current density at $|\eta| \geq 0.36$ V. The ion blocking measurements of CGO20 [18] suggest the onset of n-type electronic conductivity at $p(O_2) \approx 10^{-10}$ atm, which corresponds to the Nernst e.m.f. of approximately 0.4 V. On the other hand, polarizing at 0.36 V relates to local reducing conditions with oxygen partial pressure close to 10^{-9} atm. The fair agreement between these two $p(O_2)$ values indicates that at high overpotentials the solid electrolyte becomes a mixed conductor, at least near the triple-phase boundary. As a result, the electrode reaction may be extended to the surface of the solid electrolyte and the electrolyte ohmic drop may decrease due to the reduction of the constriction effects. Similar behavior was observed with $La(Sr)Fe(Co)O_{3-\delta}$ point electrodes in contact with CGO20 [53]. The significant activation energy for n-type electronic conductivity of CGO20 ($\sim$150 kJ/mol) suggests that much higher overpotentials should be attained for the same effect to be identified at lower temperatures.

Decreasing the operation temperature of the cell decreases the oxygen vacancy concentration in oxide electrodes, and the importance of the ionic conductivity significantly increases as shown by the polarization data at 873 K. The maximum electrochemical activity was found for the LFN and LSFC cathodes; these materials exhibit higher oxygen ion mobility than LC/LZ composites and lanthanum-strontium manganites. At the same time, the good performance of the surface-activated LFN layer at 873 K suggests that surface

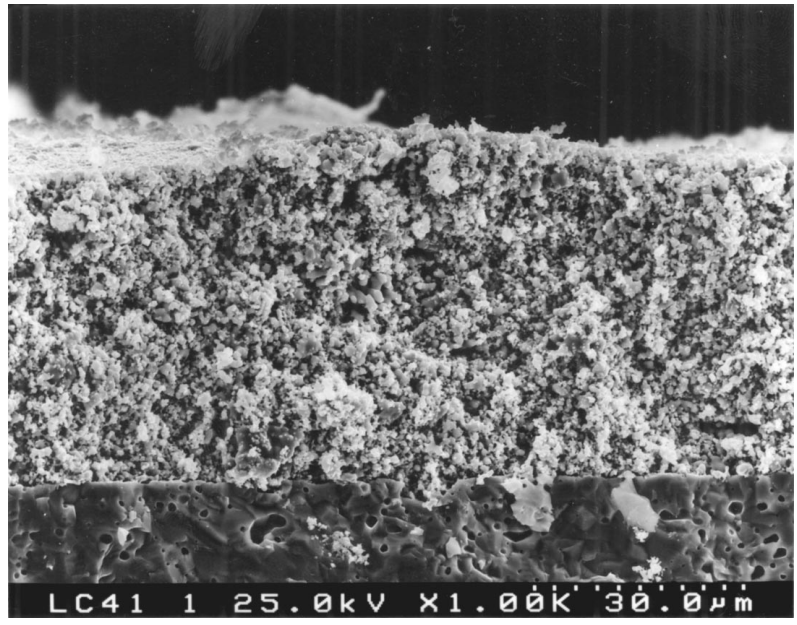

(A)

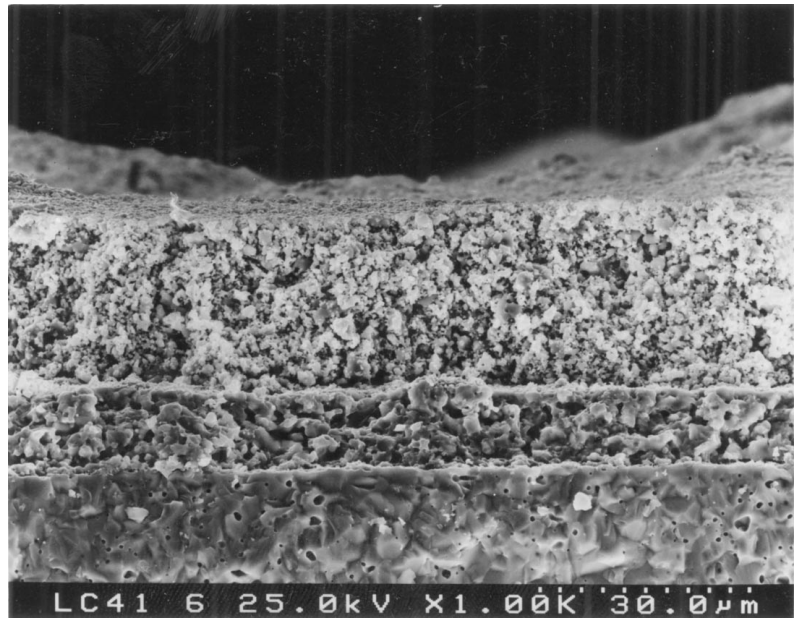

(B)

Figure 10 Cross-sectional SEM micrographs of $LaCoO_{3-\delta}$ /$La_2Zr_2O_7$ composite electrodes: (A), double layer dense plus porous; (B), single porous layer. See text for details.

kinetics continues to play an important role in the electrode behavior.

In summary, the results demonstrate an ability of significant improvement of cathode performance, which may be achieved by increasing the oxygen ionic conductivity of electrode materials (e.g. using $La_{1-x}Sr_xCoO_{3-\delta}$ in the case of composite cathodes) and further activation of the surface exchange properties (e.g. PrO_x). In addition, surface modification of ceria-based electrolytes in order to provide a higher mixed conductivity and oxygen exchange currents might also be useful.

3.7. Applications of ceria in SOFC anodes and oxygen separation membranes

Whilst the potential use of doped CeO_2 as a solid electrolyte is still questionable due to technological problems associated with easy reducibility, another promising application of ceria in high-temperature electrochemistry refers to the electrodes of SOFCs and other electrochemical cells, operating in reducing environments, and oxygen separation membranes. For applications in electrodes, an unambiguous advantage of cerium oxide is a very high catalytic and electrocatalytic activity of nonstoichimetric phases $CeO_{2-\delta}$ in redox processes (for instance, see [7, 9] and references therein). Therewith, the low electronic conductivity makes it possible to use cerium oxide only as a component of cermets or other electrode materials, but not as a single material.

As an example, Fig. 11 demonstrates an effect of surface modification of SOFC electrodes on performance of the cell, consisting of $Zr_{0.90}Y_{0.10}O_{1.95}$ solid electrolyte, $La_{0.6}Sr_{0.4}MnO_{3-\delta}$ cathode and cermet anode (76 wt% Ni, 12 wt% $Zr_{0.90}Y_{0.10}O_{1.95}$, 12 wt% CeO_2).

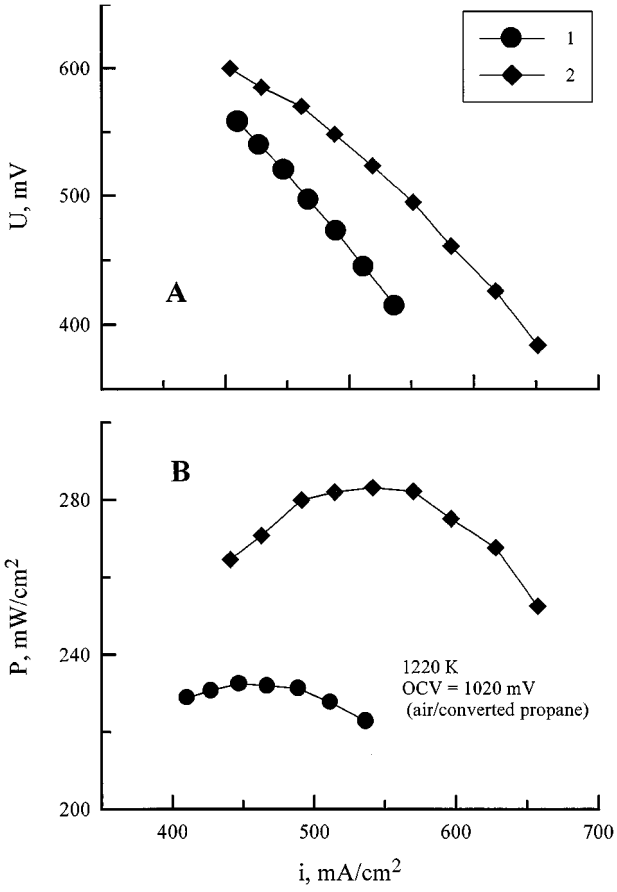

Figure 11 Dependence of voltage (A) and power density (B) on current density for a single fuel cell with $Zr_{0.90}Y_{0.10}O_{1.95}$ electrolyte (see text for details): (1), before surface modification of electrodes; (2), after surface modification of anode with cerium oxide and cathode with praseodymium oxide.

The details of the cell fabrication and testing were described in Ref. [29]. For the electrode activation, the anode and cathode were impregnated with ethanol solutions of cerium and praseodymium nitrates, respectively. After subsequent thermal treatment at 1270 K in corresponding gases, the power density of the fuel cell increased by more than 20% due to a sharp decrease of electrode polarization. In the temperature range 1150 to 1250 K, the activation of cermet electrodes with cerium oxide was found to decrease anodic overpotentials by 2–5 times.

When considering the membrane applications, one should note that oxygen permeability of ceria-based materials at membrane permeate-side oxygen pressures of 10^2–10^3 Pa is relatively low (for example, [11, 20]), whereas further reduction of this partial pressure may result in mechanical decomposition of the membrane [7, 21]. Greater oxygen permeation fluxes may be achieved by increasing the oxygen chemical potential at the membrane feed side. An increase of operating oxygen pressures is of considerable interest for film membranes, where the surface exchange limitations to the permeation flux are significant due to small membrane thickness, since oxygen surface exchange currents increase, as a rule, with increasing oxygen pressure. In addition, using electrochemical devices (high-purity oxygen generators or SOFC generators) in combination with gas turbines requires elevated pressure of exit gases for input into a gas turbine. Note that SOFC performance significantly increases at elevated pressures [54]. For fuel cells with ceria solid electrolytes, an increase of oxygen chemical potential at the cathode is expected also to enhance the stability of the electrolyte membranes [5].

In the present work, the tests of various electrochemical cells with ceria-based materials were carried out at feed-side oxygen pressures up to 100 atm; the experimental technique and equipment have been described elsewhere [55]. Testing dense CGO20 membranes with short-circuited Pt-electrodes showed an instability of platinum layers at high pressures of oxygen. For example, at 1080 K under an oxygen pressure gradient of 50 atm/1 atm, the permeation flux decreased from approximately 1.8×10^{-8} to 7.2×10^{-9} mol $\times$ s^{-1} $\times$ cm^{-2} after 20 hours of operation. Subsequent analysis of the cell showed that most of the platinum disappeared from the surface, probably due to the surface oxidation of platinum. Similar results were obtained in the course of high-pressure tests of the short-circuited CGO cells with electrodes of other materials. Most oxide electrode layers, including LSM and LSFC, exfoliated from the CGO membranes immediately after starting the tests, which can be attributed to volume changes of the electrode materials due to incorporation of large amounts of oxygen into their crystal lattice.

In contrast, testing dual-phase membranes of CGO20/LSM30 composite demonstrated sufficient stability under these conditions. No degradation of the permeation flux with time was observed at 1023 K during 100–150 h. Fig. 12 shows the dependence of the oxygen flux through LSM/CGO-1 membrane with feed-side oxygen pressures between 18 and 50 atm.

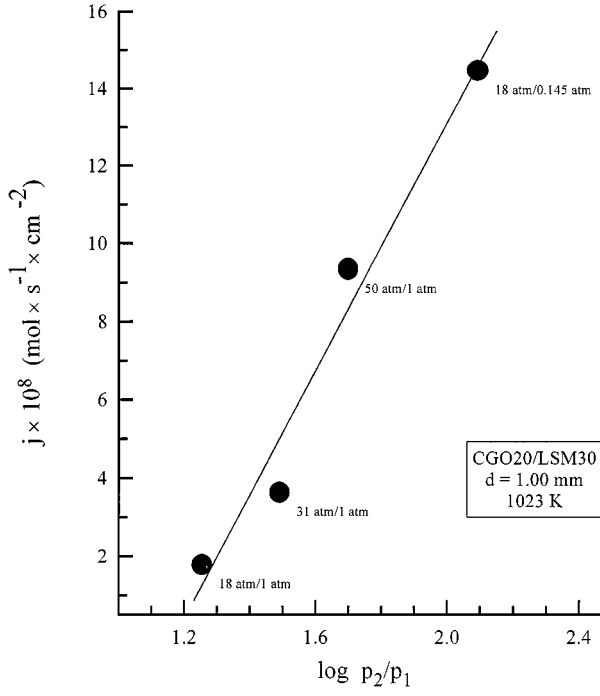

Figure 12 Dependence of oxygen permeation flux through the CGO20/LSM30 membrane on oxygen pressure gradient. The oxygen pressure values at the feed and permeate sides are marked close to the experimental data points.

The flux increases linearly with increasing oxygen partial pressure gradient, in agreement with the classical Wagner model. Under the same oxygen chemical potential gradient, the oxygen permeability of CGO20/LSM30 composites at high oxygen pressures was higher than that at low pressures. This difference could be due to an increase of the oxygen transport through the CGO phase, resulting from incorporation of excessive oxygen into the fluorite lattice of CGO and subsequent increase of the p-type conduction. In addition, placing the membranes under high pressure may also lead to formation of microcracks at the membrane surface, which does not result in open holes between membrane feed and permeate sides, but might contribute to the total permeation flux due to decreasing effective thickness of the membranes.

Therefore, using SOFCs with ceria-based solid electrolytes at high pressures requires development of new cathode materials. Use of composites consisting of CGO and perovskites, such as LSM, can be considered as a possible strategy.

4. Conclusions

The present work is devoted to a brief summary and comparative analysis of data on the electronic and ionic transport properties of gadolinia-doped ceria ceramics as well as to the electrochemical properties of different oxide cathodes in contact with ceria-based solid electrolytes. $Ce_{0.90}Gd_{0.10}O_{2-\delta}$ (CGO10) was found to possess a better stability in reducing atmospheres with respect to $Ce_{0.80}Gd_{0.20}O_{2-\delta}$ (CGO20) at temperatures below 1000 K, which makes CGO10 more suitable for intermediate-temperature SOFCs. Small additions of praseodymium oxide into CGO20 leads to a moderate increase in the stability, but the electrolytic domain boundary of the Pr-doped electrolyte is still comparable to that of CGO10. Interaction of ceria-based ceramics with electrode materials, such as lanthanum-strontium manganites, may result in formation of low-conductive layers at the electrode/electrolyte interface, thus necessitating the optimization of electrode preparation conditions. Properties of various oxide electrode materials, having thermal expansion compatible with doped ceria, are presented. A good electrochemical activity in contact with CGO electrolyte was pointed out for electrodes of perovskite-type solid solutions $La_{0.8}Sr_{0.2}Fe_{0.8}Co_{0.2}O_{3-\delta}$ and $LaFe_{0.5}Ni_{0.5}O_{3-\delta}$, and $LaCoO_{3-\delta}/La_2Zr_2O_7$ composites. Surface modification of the cathode layers with praseodymium oxide allows a considerable decrease in polarization resistance. Using highly-dispersed ceria for activation of SOFC anodes results in significant improvement of the fuel cell performance. Testing electrochemical cells with CGO20 electrolyte at high oxygen pressures (1–100 atm) showed mechanical instability of numerous perovskite electrodes as well as porous platinum layers. Composites consisting of CGO and lanthanum-strontium manganite, exhibiting a high Wagner-type permeation fluxes, can be considered for applications at elevated oxygen pressures.

Ackowledgements

This work was partially supported by the FCT (Praxis, Portugal), the Belarus Foundation for Basic Research and the Belarus State University.

References

1. B. C. H. STEELE, *Solid State Ionics* **129** (2000) 95.
2. M. MOGENSEN, N. M. SAMMES and G. A. TOMPSETT, *ibid.* **129** (2000) 63.
3. H. INABA and H. TAGAWA, *ibid.* **83** (1996) 1.
4. T. KUDO and Y. OBAYASHI, *J. Electrochem. Soc.* **123** (1976) 415.
5. M. GOEDICKEMEIER and L. J. GAUCKLER, *ibid.* **145** (1998) 414.
6. H. J. M. BOUWMEESTER and A. J. BURGRAAF, in "Fundamentals of Inorganic Membrane Science and Technology" edited by A. J. Burgraaf and L. Cot (Elsevier, Amsterdam, 1996) p. 435.
7. M. V. PERFILYEV, A. K. DEMIN, B. L. KUZIN and A. S. LIPILIN, "High-Temperature Electrolysis of Gases" (Nauka, Moscow, 1988) [in Russian].
8. D. WALLER, J. A. KILNER and B. C. H. STEELE, in "Ceramic Membranes I" edited by H. U. Anderson, A. C. Khandkar and M. Liu (The Electrochemical Society, Pennington, NJ, 1997) p. 48.
9. V. KHARTON, E. N. NAUMOVICH and A. A. VECHER, *J. Solid State Electrochem.* **3** (1999) 61.
10. T. J. MAZANEC, T. L. CABLE, J. G. FRYE and W. R. KLIEWER, US Patent 5, 306, 411 (1994).
11. V. V. KHARTON, A. V. KOVALEVSKY, A. P. VISKUP, F. M. FIGUEIREDO, A. A. YAREMCHENKO, E. N. NAUMOVICH and F. M. B. MARQUES, *J. Electrochem. Soc.* **147** (2000) 2814.
12. E. N. NAUMOVICH, V. V. KHARTON, A. V. KOVALEVSKY and V. V. SAMOKHVAL, in "Ionic and Mixed Conducting Ceramics III" edited by T. A. Ramanarayanan (The Electrochemical Society, Pennington, NJ, 1998) p. 496.
13. A. ATKINSON, *Solid State Ionics* **95** (1997) 249.
14. I. YASUDA and M. HISHINUMA, in "Ionic and Mixed Conducting Ceramics III" edited by T. A. Ramanarayanan (The Electrochemical Society, Pennington, NJ, 1998) p. 178.
15. F. M. B. MARQUES and L. M. NAVARRO, *Solid State Ionics* **100** (1997) 29.
16. A. TSODA, A. GUPTA, A. NAOUMOIDIS, D. SKARMOUTSOS and P. NIKOLOPOULOS, *Ionics* **4** (1998) 234.
17. M. HROVAT, A. AHMAD-KHANLOU, Z. SAMARDZIJA and J. HOLZ, *Mater. Res. Bull.* **34** (1999) 2027.
18. L. M. NAVARRO, F. M. B. MARQUES and J. R. FRADE, *J. Electrochem. Soc.* **144** (1997) 267.
19. A. D. S. COSTA, J. A. LABRINCHA and F. M. B. MARQUES, *J. Mater. Sci. Lett.* **15** (1996) 1716.
20. E. N. NAUMOVICH, V. V. KHARTON, A. V. KOVALEVSKY and V. V. SAMOKHVAL, in Proc. 17th Riso Int. Symp. on Materials Science, edited by F. Poulsen, N. Bananos, S. Linderoth, M. Mogensen and B. Zachau-Christiansen (Roskilde, Denmark, 1996), p. 301.
21. A. V. KOVALEVSKY, V. V. KHARTON and E. N. NAUMOVICH, *Inorg. Mater.* **32** (1996) 1230.
22. F. M. FIGUEIREDO, J. R. FRADE and F. M. MARQUES, *Solid State Ionics* **118** (1999) 81.
23. F. M. FIGUEIREDO, F. M. MARQUES and J. R. FRADE, *J. Europ. Ceram. Soc.* **19** (1999) 807.
24. F. M. FIGUEIREDO, Ph.D. Thesis, University of Aveiro, Aveiro, Portugal, 1999.
25. A. A. YAREMCHENKO, V. V. KHARTON, E. N. NAUMOVICH and F. M. B. MARQUES, *J. Electroceramics* **4** (2000) 235.
26. V. V. KHARTON, A. V. KOVALEVSKY, A. P. VISKUP, F. M. FIGUEIREDO, J. R. FRADE, A. A. YAREMCHENKO and E. N. NAUMOVICH , *Solid State Ionics* **128** (2000) 117.
27. V. V. KHARTON, A. P. VISKUP, E. N. NAUMOVICH and F. M. B. MARQUES, *J. Mater. Chem.* **9** (1999) 2623.

28. V. N. TIKHONOVICH, V. V. KHARTON, E. N. NAUMOVICH and A. A. SAVITSKY, *Solid State Ionics* **106** (1998) 197.
29. V. V. KHARTON, E. N. NAUMOVICH, V. N. TIKHONOVICH, I. A. BASHMAKOV, L. S. BOGINSKY and A. V. KOVALEVSKY, *J. Power Sources* **77** (1999) 242.
30. YU. S. GAIDUK, V. V. KHARTON, E. N. NAUMOVICH and V. V. SAMOKHVAL, *Inorg. Mater*. **30** (1994) 759.
31. F. M. FIGUEIREDO, J. R. FRADE and F. M. MARQUES, *Solid State Ionics* **135** (2000) 467.
32. V. V. KHARTON, A. P. VISKUP, E. N. NAUMOVICH and V. N. TIKHONOVICH, *Mater. Res. Bull.* **34** (1999) 1311.
33. A. A. YAREMCHENKO, V. V. KHARTON, A. P. VISKUP, E. N. NAUMOVICH, N. M. LAPCHUK and V. N. TIKHONOVICH, *J. Solid State Chem.* **142** (1999) 325.
34. V. V. KHARTON, E. N. NAUMOVICH and A. V. NIKOLAEV, *Solid State Phenomena* **39/40** (1994) 147.
35. V. V. KHARTON, V. V. ASTASHKO, P. P. ZHUK, A. K. DEMIN, A. A. TONOYAN, M. P. GILEVICH and A. A. VECHER, *Vestsi AN Belarusi, ser. khim.* **3/4** (1992) 70 [in Russian].
36. L.-W. TAI, M. M. NASRALLAH, H. U. ANDERSON, D. M. SPARLIN and S. R. SEHLIN, *Solid State Ionics* **76** (1995) 273.
37. F. M. FIGUEIREDO, J. R. FRADE and F. M. MARQUES, *Solid State Ionics*, accepted for publication.
38. D. M. BOCHKOV, V. V. KHARTON, A. V. KOVALEVSKY, A. P. VISKUP and E. N. NAUMOVICH, *Solid State Ionics* **120** (1999) 281.
39. G. M. CHRISTIE and F. P. F. VAN BERKEL, *ibid.* **83** (1996) 17.
40. D. L. MARICLE, T. E. SWARR and S. KARAVOLIS, *ibid.* **52** (1992) 173.
41. S. LUEBKE and H.-D. WIEMHOEFER, *ibid.* **117** (1999) 229.
42. J. VAN HERLE, D. SENEVIRATNE and A. J. MCEVOY, *J. Europ. Ceram. Soc*. **19** (1999) 843.
43. M. MOGENSEN, T. LINDEGAARD, U. R. HANSEN and G. MOGENSEN, *J. Electrochem. Soc*. **141** (1994) 2122.
44. J. FLEIG and J. MAIER, in "Ionic and Mixed Conducting Ceramics III" edited by T. A. Ramanarayanan (The Electrochemical Society, Pennington, NJ, 1998) p. 166.
45. H.-H. MOEBIUS, in "Extend. Abstr. 37th Meet. ISE" (Int. Society of Electrochemistry, Vilnius, 1986), Vol. 1, p. 136.
46. H. YAHIRO, K. EGUCHI and H. ARAI, *Solid State Ionics* **36** (1989) 71.
47. D. L. MARICLE, T. E. SWARR and H. L. TULLER, US Patent 5,001,021 (1991).
48. B. CALES and J. F. BAUMARD, *J. Phys. Chem. Solids* **45** (1984) 929.
49. S. LING, *Solid State Ionics* **70/71** (1994) 686.
50. B. G. POUND, *ibid.* **52** (1992) 183.
51. V. V. KHARTON, A. A.YAREMCHENKO and E. N. NAUMOVICH, *J. Solid State Electrochem.* **3** (1999) 303.
52. V. V. KHARTON and E. N. NAUMOVICH, *Russ. J. Electrochem.* **29** (1993) 1297.
53. E. MAGUIRE, B. GHARBAGE, F. M. B. MARQUES and J. A. LABRINCHA, *Solid State Ionics* **127** (2000) 329.
54. A. V. VIRKAR, K.-Z. FUNG and S. C. SINGHAL, in "Ionic and Mixed Conducting Ceramics III" edited by T. A. Ramanarayanan (The Electrochemical Society, Pennington, NJ, 1998) p. 113.
55. V. V. KHARTON, A. P. VISKUP, A. A. YAREMCHENKO, P. F. KERKO, E. N. NAUMOVICH and A. V. KOVALEVSKY, *Mater. Res. Bull*. **34** (1999) 1921.

Received 2 May
and accepted 10 July 2000